JET–P(97)44

Evidence for Volume Recombination in JET Detached Divertor Plasmas

G M McCracken, M F Stamp, R D Monk, A Meigs,
J Lingertat, R Prentice, A Starling, R Smith

JET Joint Undertaking, Abingdon, Oxfordshire, OX14 3EA,

Preprint of a paper submitted for publication in
Nuclear Fusion

November 1997

Abstract.

Evidence for volume recombination in the JET divertor has been obtained from the population ratios of the excited states of neutral hydrogen. The ratio of the Balmer series lines $D_\gamma D_\alpha$ has been used to identify recombination at both the inner and the outer divertor target. At the outer target the onset of recombination is well correlated with the plasma detachment as observed with Langmuir probes in the divertor target. While T_e obtained from the target probe characteristics falls to ~2eV, T_e from the population distribution of the excited states is 0.8±0.1 eV. The peak plasma density looking across the outer divertor leg just above the target exceeds $2.5x10^{20}$ m^{-3}. When the plasma becomes partially detached from the outer target the radial distribution of recombination shows a maximum close to the outer divertor strike point.

I. Introduction

In tokamak divertors the plasma density frequently rises to values $\geq 10^{20}$ m^{-3} and the electron temperature, T_e, falls to ~1 eV. Under such conditions recombination of ions and electrons can occur. This recombination is thought to play an important role in reducing the incident ion flux and detaching the plasma from the divertor target [1,2,3,4]. The distribution of the populations of excited states of hydrogen in a plasma depends on both excitation and recombination processes. Excitation tends to preferentially populate the low-lying excited states and recombination the upper ones. Thus the process of recombination may be identified from the ratio of the excited state populations, particularly in the Balmer series [4,5,6]. Understanding the plasma behaviour under these conditions can be further complicated by the plasma becoming opaque to the emitted radiation, particularly the Lyman alpha radiation [1]. The Balmer lines are much less affected by self absorption under the plasma conditions of interest [7] but the population distribution of the upper excited states can be changed by the opacity of the plasma to the L_α radiation.

In the present paper we first discuss the expected emissivity due to the different processes, section II, and then present experimental observations of the emissivities of the hydrogen Balmer series in the JET divertor. With increasing main plasma density a reduction in the divertor D_γ/D_α and D_δ/D_α ratios is observed in the density range where excitation dominates, showing an increase in density, and then a large increase in the ratios occurs which is attributed to the onset of recombination and correlated with detachment.

II. Atomic physics.

The measurement of the population levels has been discussed as a diagnostic technique by a number of authors [1,8,9] including notably Fujimoto [10], who has used the ratios of the excited states, n=3-> 2, n=4-> 2, n=5-> 2, to estimate the electron density. These lines of the Balmer series are in the visible and are readily observed spectroscopically. The results of calculated ratios based on excitation models are shown in fig 1. Similar curves are available for the Lyman series in the vacuum ultraviolet. It is seen that over the density range $n_e=10^{17}$ to 10^{21} m^{-3} the ratios vary by over an order of magnitude, with the ratio of the higher lying states varying more than the lower ones. Except at very low temperatures the dependence on T_e is small.

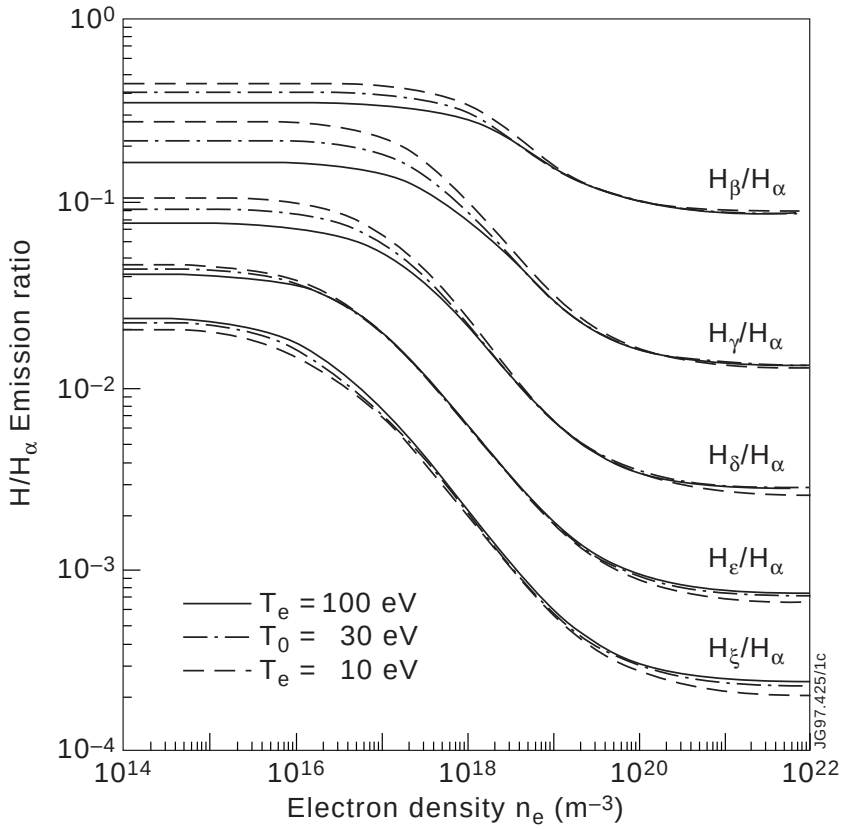

1. Calculated density dependence of the emission line intensity ratios H_β, H_γ, H_δ, $H_\varepsilon$and H_ζ to H_α. The plasma is assumed to be at high temperature in the ionizing phase and optically thin. From Fujimoto et al [10].

The situation becomes more complicated when recombination is taken into account. This has been considered recently for experimental data from C-Mod by Terry at al [5,6], JET [4], ASDEX Upgrade [11] and DIIID [12]. The photon emissivity coefficients (PECs), which incorporate models of the balance between the excited states, are available for excitation and recombination separately in the ADAS data base [13]. The excitation data from ADAS have been compared to the Fujimoto calculations and the recombination data has been compared with the population ratios calculated by Terry. In both cases good agreement was obtained.

The absolute emission due to recombination depends approximately on n_e^2 while the emission for excitation depends on the product $n_e n_o$, where n_o is the neutral density. Thus the ratio of the emission for recombination to excitation depends on the ratio n_e/n_o. An example of the emission rates for H_α as a function of T_e with $n_e=1x10^{20}$ m^{-3} and various values of n_o is shown in fig 2. Because of the steep decrease of the excitation rate at low temperature recombination only becomes dominant for $T_e < 1.5$ eV, for any reasonable value of n_o. Similar curves exist for H_γ with the cross-over shifted to slightly higher T_e.

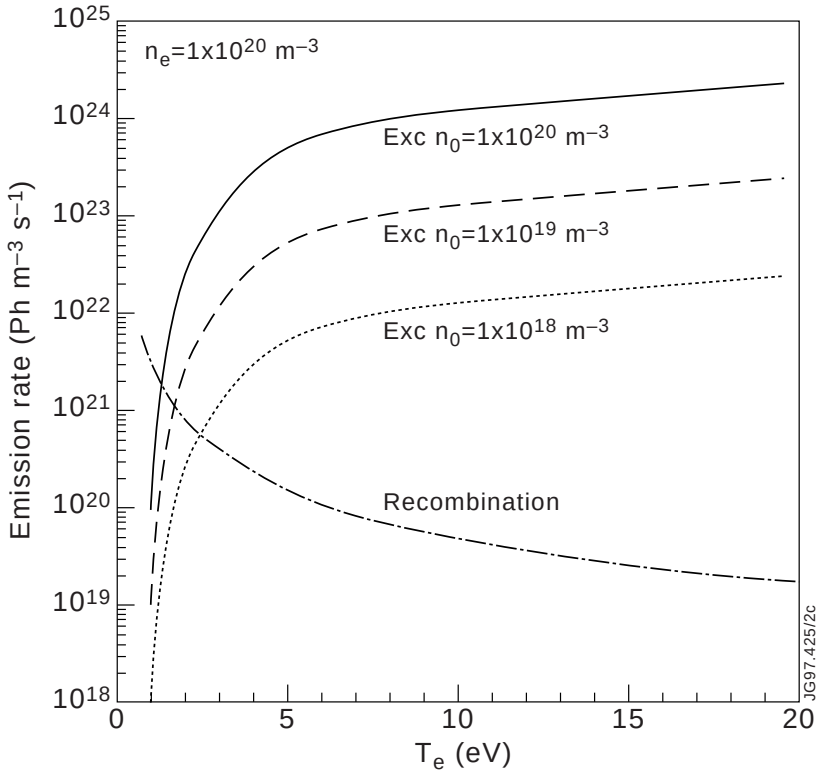

2. H_α emission rates due to excitation and recombination for an electron density $n_e=10^{20}$ m^{-3} from ADAS [13]. The excitation rates are calculated for 3 different neutral densities.

The ratio of H_γ/H_α emission rates for excitation and recombination are shown as a function of temperature in fig 3. The large difference between the recombination and excitation ratios is clearly observed. For recombination the populations of the high-lying excited states are much larger than for excitation, the ratio of H_γ/H_α emission ratios varying from 0.18 at $n_e=2x10^{19}$ m^{-3} to 0.10 at $n_e=10^{20}$ m^{-3} for a plasma temperature of Te = 1eV. The small variation with temperature of the H_γ/H_α ratio due to excitation is also observed in fig 3. The variation of the ratio for recombination, due to both T_e and n_e changes, is more marked.

Other recombination mechanisms have also been discussed [7,14]. The contribution due to radiative recombination has recently been calculated by Behringer and shown to be small [7]. Molecularly assisted recombination (MAR) has been discussed by Pigarov and Krasheninnikov [14]. Although the recombination rate coefficients are much larger than for 3-body recombination,

the absolute rates cannot be determined as the density of the vibrationally excited molecules, on which the process depends, have not been measured. Experimental evidence for MAR has been sought in C-Mod but not yet found, while 3-body recombination is in good agreement with experiment [5].

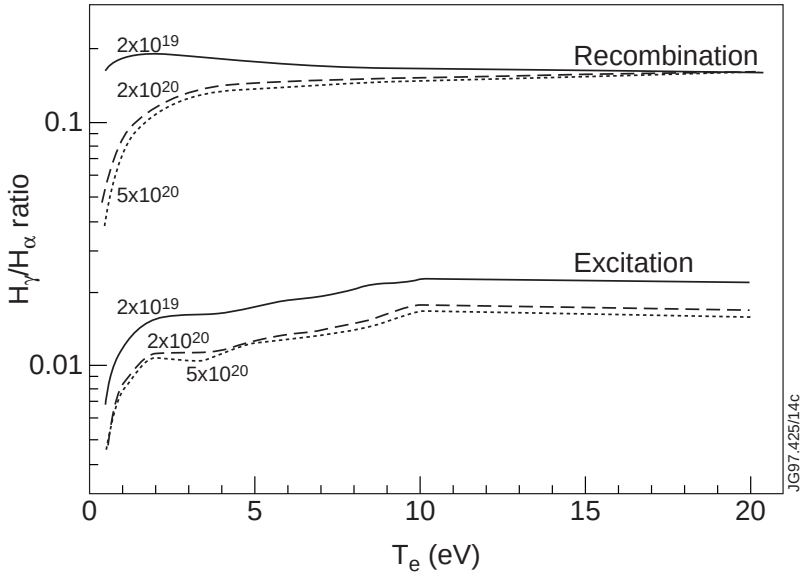

3 Line intensity ratios calculated from ADAS photon emissivity coefficients (PECs) for H_γ/H_α for electron excitation and for recombination at three different densities [13]; $n_e=2x10^{19}\ m^{-3}$, $n_e=2x10^{20}\ m^{-3}$and $n_e=5x10^{20}\ m^{-3}$.

The effect of self absorption of the emitted radiation by the plasma has been shown to be significant by Behringer. For example, for a plasma cylinder of 50 mm radius, at $n_e=5x10^{19}\ m^{-3}$ and Te = 1eV the escape probability for Lyman alpha radiation is <5%. While the Balmer series lines are not significantly attenuated under the conditions of interest the absorbed L_α radiation can significantly alter the populations of the upper states [15]. Fortunately for present purposes the ratio of the populations of the n=3, 4 and 5 levels is not significantly altered [7].

III. Experimental Data.

III.1. Outer Divertor Target.

Spectroscopically resolved data in the visible are available from integrated views of both the inner and outer JET divertor targets and from 7 narrower angle views (30 mm wide at the target) (KS3). In addition there are 12 tracks across the outer target each 13 mm wide, spectrally resolved over the range 400 to 700 nm. (KT3B). KS3 is a survey instrument and routinely monitors D_α, (656.27 nm), D_β, (486.13 nm) and D_γ (434.05 nm). KT3B can monitor D_β, D_γ and D_δ (410.17 nm) simultaneously. The lines of sight are shown in fig 4. The D_α spatial distribution across the inner and outer target is obtained, with 3 mm resolution at the target, from a flux camera with an interference filter, (KL2). .

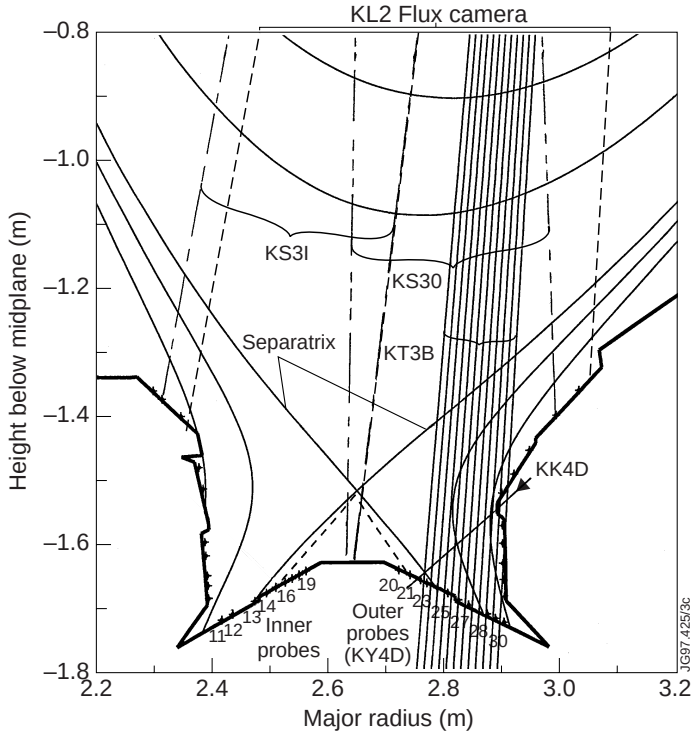

4. Lines of sight of the two visible spectrometer diagnostic systems KS3 and KT3B, the flux camera, KL2, the divertor interferometer, KG6D and the ECA diagnostic, KK4D and the divertor target probes.

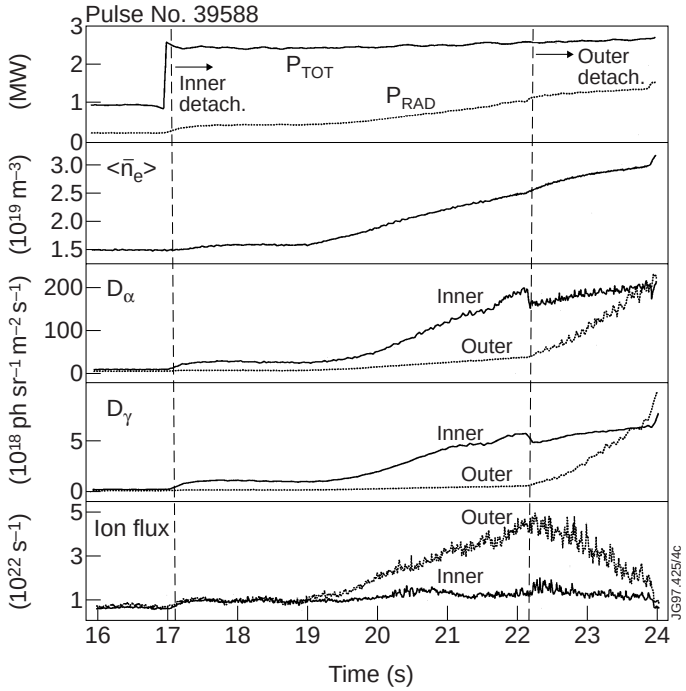

5. Global parameters for the 2MW L-mode density limit shot# 39588. The total emission from D_α and D_γ spatially integrated over the inner and outer targets and the total integrated ion current to the probes are compared.

Results for a 2 MW L-mode density limit shot with a horizontal divertor target (# 39588) are shown in figs 5 and 6. The global parameters of the shot are shown in fig 5. Detachment from the outer target is clearly seen at ~22.1 s by the drop in the total ion current to the target. In fig 6 the intensities

of D_β , D_γ and D_δ from KT3B have been compared to D_α from KS3 outer along the same line of sight (R=2.833 m). The difference in the three ratios is quite marked. At low density they are all consistent with the theoretical values from fig 1 for a density, n_e~2x10^{19} m^{-3}. As the central density, n_e, rises the ratios decrease, indicating that the density near the target increases to ~1x10^{20} m^{-3} at 22 s. An independent measure of the density at the outer divertor is obtained from the divertor interferometer, KG6D , which has a line of sight across the flux surfaces, as shown in fig 4. As the measurement is of the line integral density a rough estimate of the peak density can be obtained by dividing by the density e-folding length, obtained from the target probe data (KY4D), ~0.06m. Using the JET divertor Electron Cyclotron Absorption (ECA) diagnostic [16], the upper cut-off frequency for the ECE extraordinary mode can be measured and this also determines the peak density along the line of sight. This measurement is also plotted in fig 6. The peak densities from the ECA system and the interferometer are in good agreement with each other and with the density measured by the probes up to the point of detachment, and the absolute density is within a factor of 2 of the density derived from the D_γ/D_α ratio.

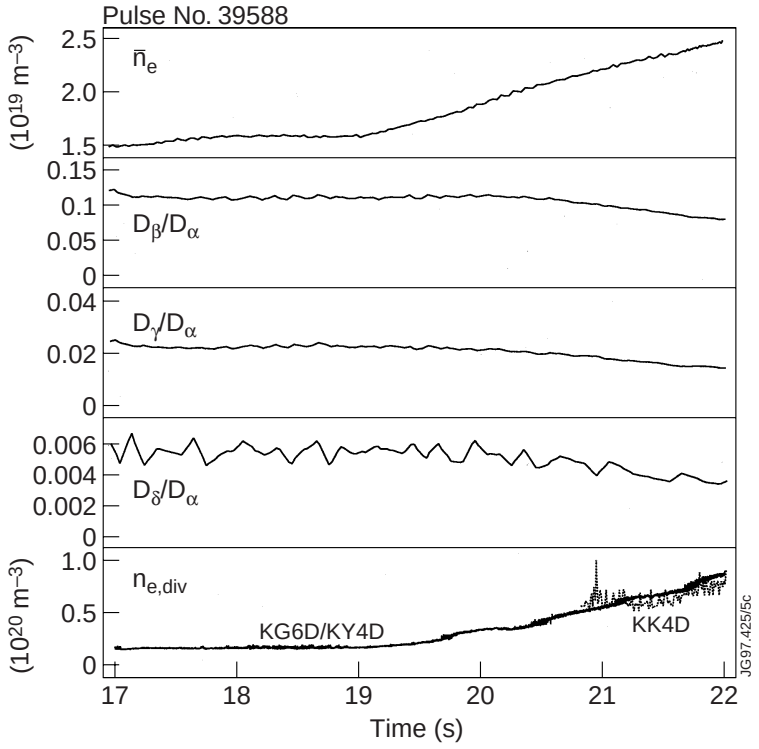

6. Variation of the line integrals of the ratios D_β/D_α, D_γ/D_α and D_δ/D_α from KS3 and KT3B during a density ramp in shot # 39588 at a major radius R=2.833 m. The maximum densities along the line of sight, derived from the divertor interferometer and the ECA diagnostic (cf fig 4) are also shown, (see text).

The local D_α signal used in fig 6 saturates at ~22s. Looking at fig 5 it is seen that at this time the absolute values of the integrated D_α and D_γ signals continue to rise. Using the spatial integrals across the outer target, which have a larger dynamic range than the local lines of sight, the D_γ/D_α ratio is plotted in fig 7. The decrease in the D_γ/D_α ratio at the outer target up to 22 s,

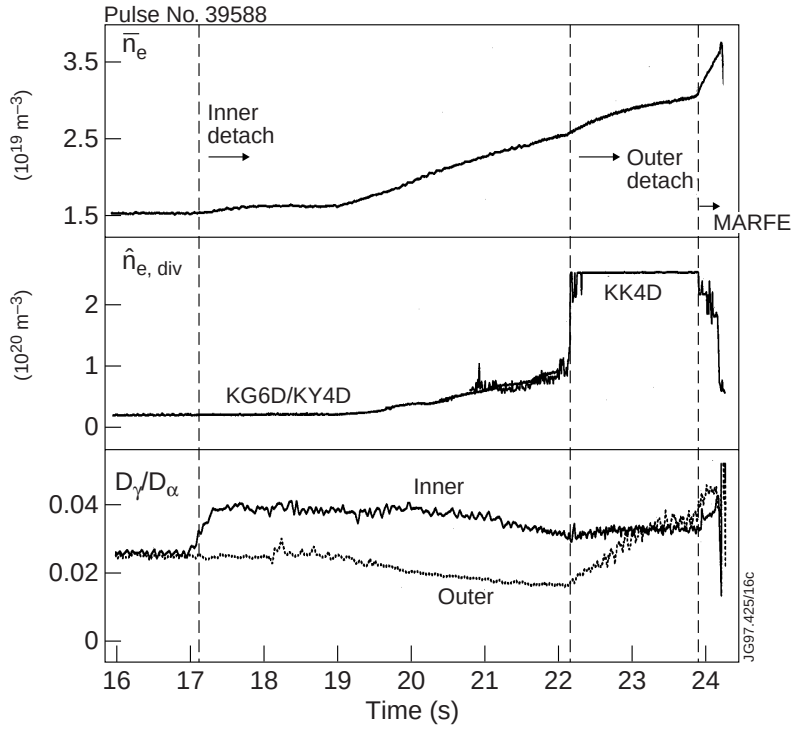

7. The D_γ/D_α ratio for the integrated views of the inner and outer target of KS3. The sudden rise of the D_γ/D_α ratio, indicating the onset of recombination occurs at the inner target at significantly lower density than the outer target. Shot 39588 .

indicating the increase of density in the excitation only situation, is again clearly observed and then there is an abrupt change in the D_γ/D_α ratio at the outer target, coincident with the onset of detachment. Although the divertor interferometer fails at 22s the ECA system continues to make measurements. This shows that the peak density along the line of sight in the divertor rises abruptly and exceeds $2.5 \times 10^{20}\ m^{-3}$. Beyond this level the diagnostic cuts off, but is still showing that the density is above the cut-off. At the same time the density measured by the probes at the target falls indicating that the region of maximum density is starting to move towards the x-point. It is also observed that the density measured by ECA diagnostic falls again at 23.9s, just before the plasma disrupts. This is because the region of peak density now moves further away from the line of sight of the ECA diagnostic, towards the x-point, at this stage. The same effect is observed with the bremsstrahlung distribution as discussed in section III.2.

The rise in the D_γ/D_α ratio is modest compared with the value of the ratio expected when recombination is dominant. This is due to recombination being localized within the field of view, as will be discussed in the next section.

III.2. Spatial Distribution of Excited States

The spatial variation of the D_γ and D_α has been obtained using data from the flux camera and the KT3B spectrometer. The spatial calibrations of the two diagnostics were cross checked using a

peaked CII distribution and a 15 mm correction applied to the spectrometer. The spatial distribution of the D_α, D_γ and D_δ are compared in fig 8 for 3 different times in shot 39588. At 18.5 s the distributions are fairly flat for all 3 species giving a D_γ/D_α ratio of ~0.02 over the range R= 2.75 to 2.9 m. This is consistent with excitation only and a density of ~2×10^{19} m^{-3}. At t=21.5 s all 3 intensities have increased but the D_α has peaked at ~2.80 m resulting in a decrease in the D_γ/D_α and D_δ/D_α ratios, indicating a density increase there, but with the radiation still due only to excitation. At 23.5s the D_γ and D_δ radiation have changed dramatically, increasing at small major radius, and the D_γ/D_α ratio now increasing to ~0.10. Referring to fig 3 we see this is consistent with recombination becoming dominant. If it is assumed that the radiation is all due to recombination then it is possible to estimate the local T_e from the ratios of D_γ/D_α and D_δ/D_α [6]. The experimental values of these ratios at the peak radiation are D_γ/D_α =0.08 ±0.01 and D_δ/D_α =0.025±0.005. Comparing with the ADAS photon emissivity coefficients these results are both consistent with T_e=0.7 to 0.9 eV at a density $n_e=2\times10^{20}$ m^{-3}. Assuming a higher density would result in a slight increase in the value of T_e deduced.

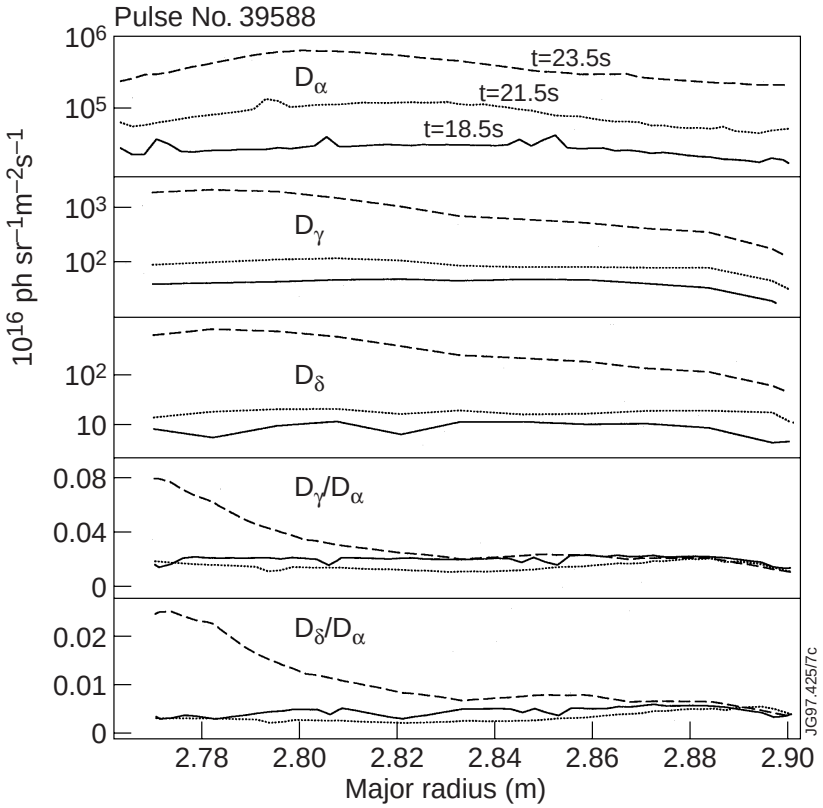

8. The spatial distribution of the line ratios D_γ/D_α and D_δ/D_α for the 12 chords corresponding to the lines of sight of the KT3B spectrometer looking at the outer target, cf fig 4. The D_γ and D_δ intensities are obtained from KT3B and D_α from the flux camera KL2. Shot 39588 @ 18.5 s, 21.5 s and 23.5 s.

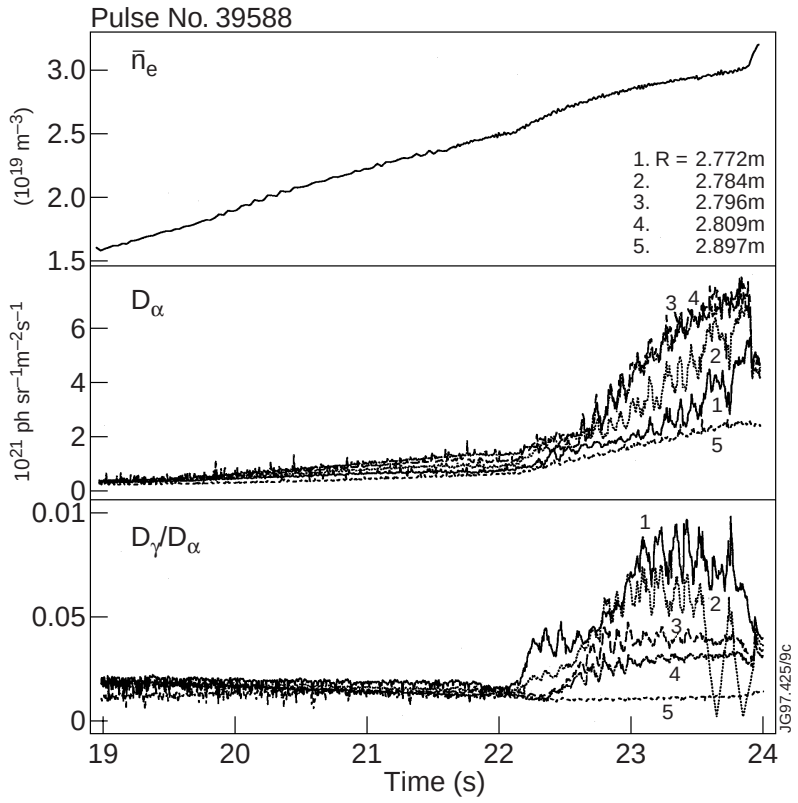

9 Time dependence of the chords of D_α signal and of the ratio $D_\gamma D_\alpha$ for five spatial channels of KT3B.

The time dependences of these signals are shown in fig 9. It is noted that channels 1and 2 respond first at 22.2s, channel 3 and 4 are a little later at 22.3s. The ratio does not rise for R>2.82 m indicating that the radiation in these channels is still predominantly due to excitation, at a density of $n_e \approx 5x10^{19}\ m^{-3}$. The absolute value of the D_γ intensity is very similar for channels 1, 2 and 3, but is ~30% lower for channel 4. The absolute value of the D_α radiation is a maximum for channels 3 and 4. Recombination appears to dominate for the 2 inner channels and then decrease in importance. Note however that the outermost channel in fig 9 intersects the wall outside the vertical target and therefore relates to the plasma above z=-1.50 m (cf fig 4.). There is no indication of recombination on this channel, as expected. Referring to fig 4 the maximum recombination is near the major radius of the outer target strike point. This is consistent with the results from C-Mod [5], though in our case we cannot determine the vertical height of the recombining region.

An interesting survey of the position of the different radiating species is obtained from the flux camera KL2 as shown in fig 10. Here the CII (λ=657.8 nm), and the D_α radiation (λ=656.3 nm) are shown in contour plots as a function of time. Detachment at the inner target occurs at 16.2s as discussed in the next section. Before 22s the radiation from both species at the outer target is clearly in the SOL, radially outside the strike point (R=2.76 m). When the plasma detaches from the outer target the CII radiation abruptly jumps towards the x-point position (R=2.62 m) and broadens, as viewed

radially from the top. Referring back to fig 4 it is seen that this is consistent with the radiation moving upwards along the separatrix. This behaviour is expected to occur as T_e at the target falls. The D_α radiation does not move as much radially but the radial profile gradually broadens. At 24s, just before the disruption, the CII and the D_α radiation become strongly peaked at the x-point position. The bremsstrahlung (not shown) also peaks strongly at the x-point radius indicating high density there. It has been already noted that the density above the target, measured by the ECE absorption diagnostic, falls at this time, cf fig 7.

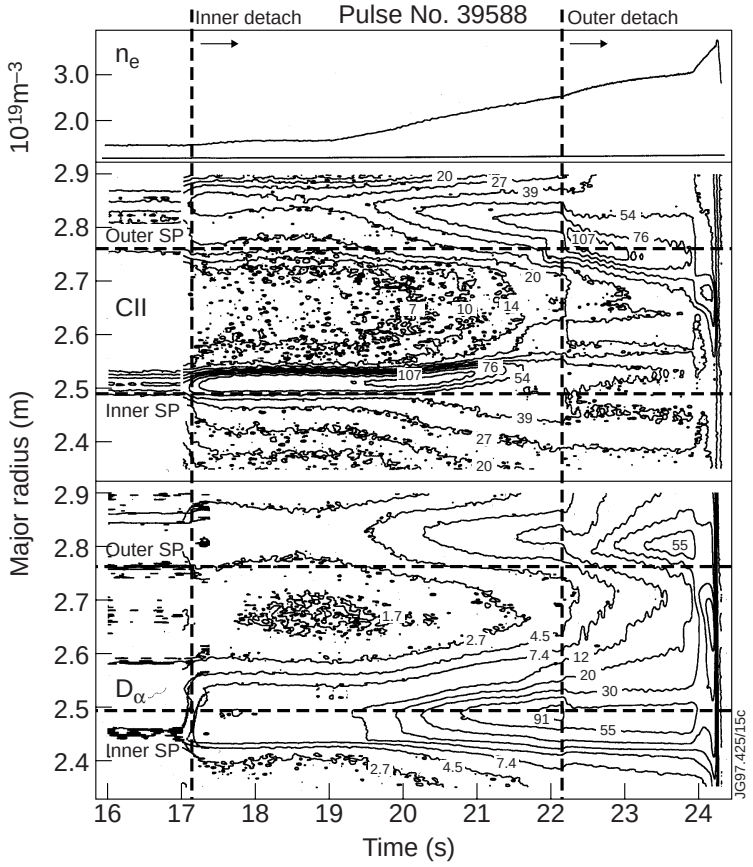

10. Spatial distributions of the CII (λ=657.8 nm), and the D_α radiation (λ=656.3 nm) from the KL2 camera are shown as contour plots. The radial position of the inner and outer strike points and the x-point, as viewed by the camera are shown. The times of detachment at the inner and outer targets, as determined by the D_γ/D_α ratio (cf fig 7), are also shown. The contour plots are in units of 10^{18} photons m^{-2} s^{-1} for CII and 10^{20} photons m^{-2} s^{-1} for D_α.

III.3. Inner Divertor Target.

The only visible spectrometer viewing the inner target is KS3. In general only the integrated views over the whole target are available for the D_γ signals. Thus the signals are averaged over the volumes where there is recombination and those where there is only excitation, leading to a smaller increase in the D_γ/D_α ratio than could be expected if recombination dominated, as was seen for the outer target, fig 7. Nevertheless, a clear onset of recombination can be observed in shots where there is a density scan. The spatially integrated D_γ/D_α ratio is shown for both the inner and outer targets for

the L-mode shot in fig 7 and for an ohmic shot (#36854) in fig 11. For the ohmic shot the D_γ/D_α ratio rises at 13.0 s for the inner target, corresponding to a core density of $\bar{n}_e=1.8\times10^{19}$ m^{-3}, and at ~15.5 s for the outer target, corresponding to $\bar{n}_e=2.9\times10^{19}$ m^{-3}. For the L-mode shot the inner target shows D_γ/D_α ratio rising at 17s ($\bar{n}_e=1.5\times10^{19}$ m^{-3}) and the outer target rise occurs at 22s ($n_e=2.5\times10^{19}$ m^{-3}). These results are consistent with the data from the target probes which show that the onset of detachment occurs first at the inner target. The absolute rise in the D_γ/D_α ratio is about the same in both inner and outer targets.

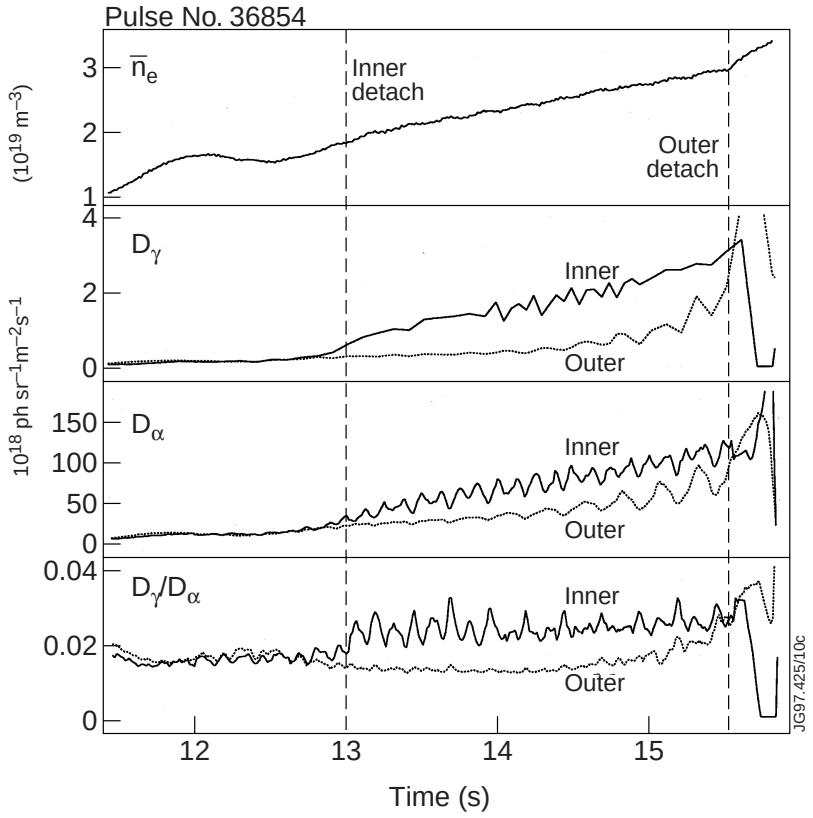

11. The D_γ/D_α ratio for the integrated views of the inner and outer target of KS3 for an ohmic discharge, #36854. As in fig 7 the sudden rise of the D_γ/D_α ratio, indicating the onset of recombination occurs at the inner target at significantly lower density n_e, than the outer target. The oscillation on the signals is due to a small amplitude, 4 Hz, scan of the strike point position.

The inner detachment is shown very clearly in the contour plots from the KL2 camera, fig 10. Before 17 s the D_α radiation is located outside the strike point. At 17.2 s, coincident with the time the D_γ/D_α ratio rises (fig 7), the radiation from the CII, and the D_α broaden markedly, consistent with the measured fall in the plasma T_e at the target (see section 4). Much of the D_α radiation appears to be coming from the region between the separatrix and the inner wall, in good agreement with the 2-D fluid modelling of JET by Borrass et al [17]. The CII radiation is coming from the region above the private flux zone. The intensities increase as the density increases, with the CII radiation moving towards the x-point. Just before the plasma detaches

from the outer target the intensities decrease and at the outer detachment all the radiation bands broaden. Very similar behaviour was observed in the ohmic discharge. However in this case a MARFE forms as soon as the plasma detaches from the outer target and after 17.8 s it moves rapidly up the inside wall of the tokamak. It would appear that the additional power in the L-mode discharge stabilizes the detachment.

III.4. Correlation with Target Langmuir Probe Data.

The data from the probes in the target characteristically show an indication of detachment, with the ion saturation current falling as the core density increases towards the density limit and T_e falling below 5 eV. The total ion current to the inner and outer targets was shown in fig 5 and indicated detachment at the outer target, with an abrupt fall in the current at 22.2s corresponding to the divertor MARFE. At the inner target, J_{sat} from the probes indicates detachment occurring near the corner of the divertor, as previously observed in ohmic discharges with horizontal target [18]. This behaviour is also predicted by fluid modelling of JET [17]. The temperatures for 6 individual outer target probes (23 to 28, cf fig 4) are compared in fig 12. At 19 s the temperature decreases with increasing major radius from probe 23 near the strike point (R=2.761) to probe 28 (R=2.861). As the density increases the temperature drops to less than 5 eV for probes 23-25 while staying almost constant for probe 28. No such consistent decrease in T_e is observed to coincide with detachment at the inner target at 17 s in the L-mode shot #39588. This is not understood at present. However the decrease in T_e and in J_{sat}, coincident with the rise in the D_γ/D_α ratio at the inner target, is observed in the ohmic shot #36854.

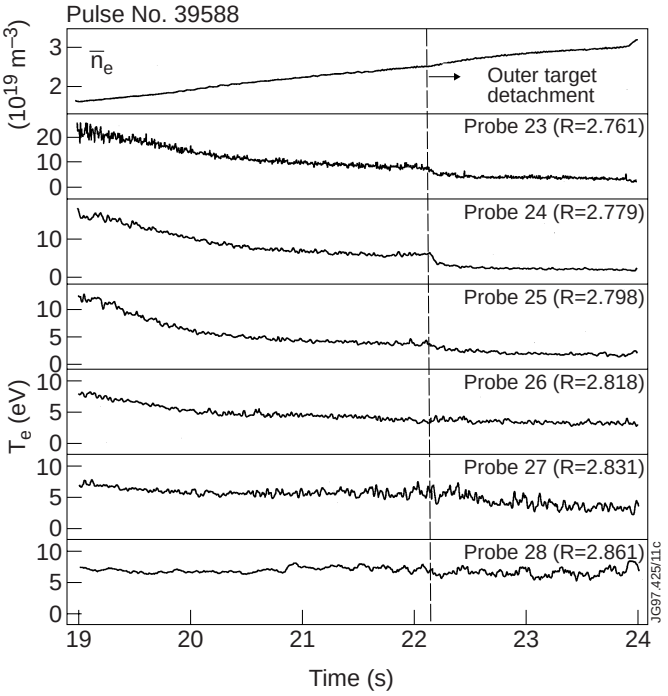

12. Time dependence of T_e from the outer target probes 23 to 28 (R=2.761 m to 2.861 m) showing detachment at 62.1 s

The time dependence of J_{sat} at the probes has been compared with the D_γ/D_α ratio in fig 13 for same radii. Because the vertical height of the D_γ and D_α radiation above the target is uncertain it is difficult to determine which flux surface to connect the probes to, and so we have simply compared the two signals at the same major radius. The jump in the D_γ/D_α ratio occurs as T_e drops to ~3 eV and the drop in the ion current is well correlated with the increase in the D_γ/D_α ratio . The correlation is even clearer in fig 14a where the D_γ/D_α ratio is plotted against T_e for 3 probes. It is noticeable that the D_γ/D_α ratio decreases as T_e falls. This is expected for the excitation radiation, cf fig 3. In fact the D_γ/D_α ratio is expected to decrease both as a consequence of the density increasing and the T_e decreasing. At ~ 3 eV the D_γ/D_α ratio starts to increase and it reaches its maximum value at 2 eV. The increase is larger for the probes close to the strike point indicating that for these chords the radiation is increasingly recombination dominated, as was seen in fig 8. The electron temperatures used have been derived from single probes using the virtual asymmetric double probe fit [19]. This model attempts to compensate for the low ratios of the electron to ion saturation current that are typically observed in the high recycling conditions [20]. Using the conventional single probe exponential fit the derived electron temperature saturates at ~ 3 eV compared to the ~ 2 eV derived with the asymmetric double probe fit. However the derived temperature may still be overestimated due to plasma resistivity [21] and kinetic effects. [22].

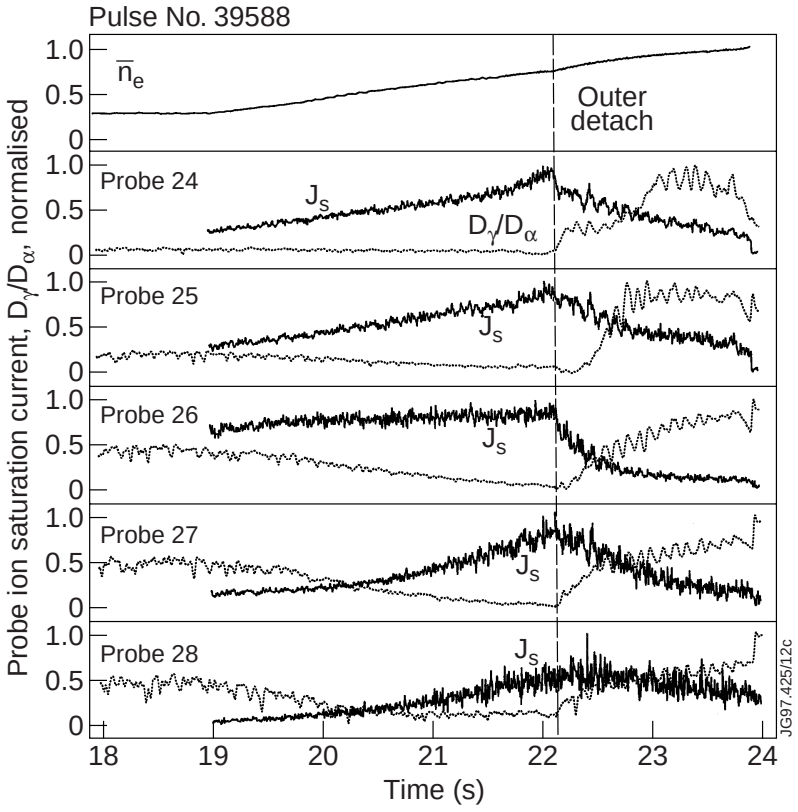

13 Correlation of the ion saturation current, J_{sat}, from the outer target probes, 23 to 28, with the value of the D_γ/D_α ratio from KT3B/KL2B at the same major radius.

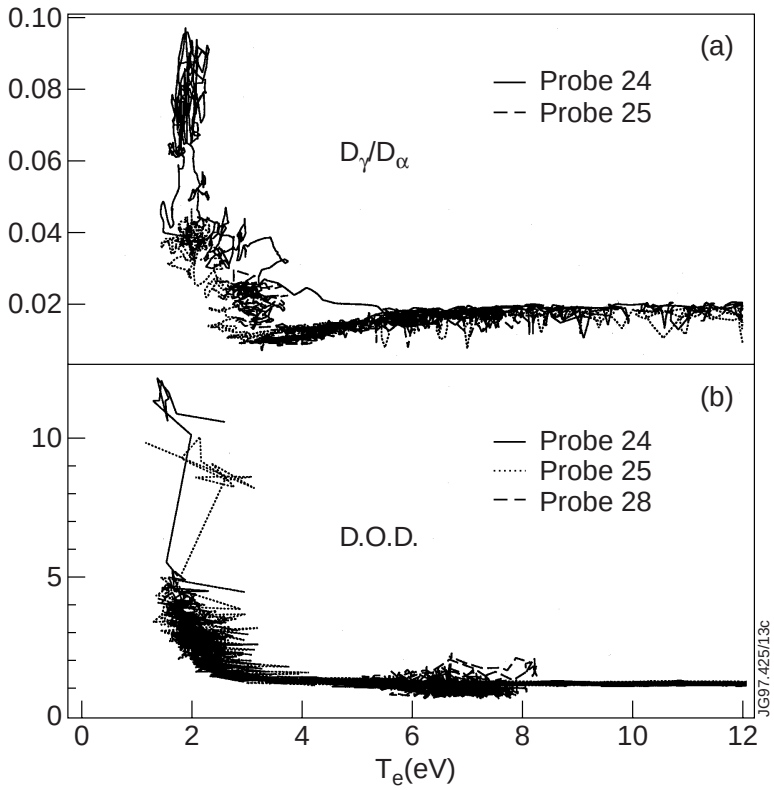

14. (a) D_γ/D_α ratio, obtained from KT3 and KL2, at two different major radii plotted against probe measured T_e at the same radius.

(b) Degree of Detachment (D.O.D.), defined in eqn(2), from 3 probes, plotted against T_e measured by the probes.

Using the simple "two-point" model [23] of the divertor scrape-off layer it can be shown that the ion flux (I_{div}) to the divertor should approximately scale according to :

$$I_{div} = n_{div} c_{div} = \frac{7\gamma L_c}{8\kappa_o m_i} \frac{n_{mid}^2}{T_{mid}^{3/2}} \qquad (1)$$

where γ is the sheath transmission coefficient, κ_o the electron thermal conductivity coefficient, m_i the ion mass, L_c the connection length and the subscripts *div* and *mid* refer to the divertor and midplane respectively. Assuming the $n_{mid} \propto \bar{n}_e$ then the Degree of Detachment (D.O.D.) [24] may be defined as follows:

$$D.O.D. = \frac{I_{div}^{scal}}{I_{div}^{measured}} = \frac{C\,\bar{n}_e^2}{I_{div}^{measured}} \qquad (2)$$

such that we define D.O.D. > 2 as the threshold for the onset of detachment to occur. The D.O.D. definition has been shown to be comparable to the measured electron pressure drop between the

SOL and the divertor [24]. Thus it serves as a useful definition to quantitatively determine detachment from the divertor probe measurements. The D.O.D. has been calculated for the outer divertor target probes. Plotting D.O.D. vs local plasma temperature T_e, fig 14b, it is seen that there is very similar behaviour of the DOD and the D_γ/D_α ratio, illustrating that detachment and recombination are closely related. The plasma is attached (D.O.D. =1) at the outer target for all temperatures down to 3 eV. At T_e= 3eV, as measured by the probes, the D.O.D. begins to rise coincident with the rise in the D_γ/D_α ratio. In earlier assessments of detachment the question was posed [25], can detachment be explained by momentum transfer via ion and neutral collisions [25,26]? The present results indicate that on JET there is no sign of detachment until recombination sets in. Ion-neutral friction, if it plays a role in detachment, would only be effective once volume recombination has started to occur - perhaps by slowing the plasma flow sufficiently to permit the recombination to be effective in reducing the plasma flux to the target [27].

IV. Conclusions

Conclusive evidence of recombination near the divertor target in high density JET discharges has been obtained from comparison of experimental measurements of the D_γ/D_α ratio of the hydrogen Balmer series with atomic physics calculations. At the outer target the recombination is strongly correlated with the rollover of the ion saturation current, determined by the probes in the target plate. At a measured temperature of ~3 eV the ion saturation current to the plate falls and recombination radiation suddenly dominates the Balmer series emission. As the probe temperature measurements are uncertain, due to kinetic and other effects, we consider the T_e value to be an upper limit. Assuming that recombination is the main source of radiation the D_γ/D_α and D_δ/D_α ratios indicate local values of T_e in the range 0.7 to 0.9 eV. Comparison of the absolute emission rates indicates that conventional three-body recombination only dominates for T_e <1.5 eV, for any reasonable value of neutral density. The peak plasma density on a sight line just above the outer target has been measured using the electron cyclotron cut-off frequency and shown to be greater than $2.5\text{x}10^{20}$ m^{-3}.

Spatially, recombination occurs near the outer strike point. At larger major radius, away from the separatrix, the radiation is still predominantly due to electron excitation. The onset of recombination is directly correlated with the onset of detachment, determined by the rollover of the ion saturation current measured at each of the probes in the outer target plate. This correlation appears to indicate that recombination is the dominant mechanism determining detachment. While the original proposal that momentum transfer to neutrals is not entirely ruled out it seems likely that it plays only a subsidiary role. When detachment occurs, the radiation sources of CII, D_α and the bremsstrahlung move up towards the x-point and just before the formation of the x-point MARFE the density in the divertor region falls.

At the inner target the experimental measurements have less good spatial resolution and the position where recombination occurs cannot be so well established. Nevertheless, from the spatially integrated views it is clear that the D_γ/D_α ratio increases to a similar value to that observed at the outer target. The CII and D_α radiation and the bremsstrahlung sources move up towards the x-point in a similar fashion to that at the outer target plate. The recombination occurs at lower values of n_e consistent with the inner target plasma being characterized by a lower temperature and higher density than the outer target.

Measurements of the D_γ/D_α ratio have been shown to be a simple and effective way of determining the onset and the spatial distribution of detachment. Further exploitation of the technique is clearly warranted.

Acknowledgements.

We are grateful to L D Horton, P C Stangeby, K Borrass and C Maggi for valuable discussions and helpful comments on the text.

References

1. Post, D E, J Nucl Mater.220-222 (1994) 143

2. Krasheninnikov, S I, Phys Plasmas, 4 (1997)1638

3. K Borrass, J Nuclear Materials, 241-243 (1997) 250

4. Loarte, A, J Nuclear Materials, 241-243 (1997) 118

5. Lumma, D, Terry, J L, and Lipschultz, B , Phys Plasmas, 4 (1997), 2555.

6. Terry, J L, Lipschultz, B , Lumma, D, et al in Controlled Fusion and Plasma Physics (Proc 24th Eur Conf, Berchtesgaden 1997), Vol 21A, Pt xx, European Physical Society Geneva (1997) 573.

7. Behringer, K, Max Planck Institut fur Plasmaphysik, Report 10/5 , Feb 1997. "The influence of opacity on hydrogen line emission and ionization balance in high density divertor plasmas".

8 Johnson, LC, and Hinnov, E, J. Quant. Spectr. Rad. Transf. 13, (1973) 33.

9. Stamp, M F, and Summers, H, Plasma Physics and Controlled Fusion Vol 14B, Pt III (1990), 1377. (Proc 17th Eur. Phys. Soc Conf., Amsterdam)

10. Fujimoto, T, Miyachi, S, and Sawada, K, Nuclear Fusion 28 (1988)1255

11. Napiontek, B, Wenzel, U , et al., P4.007, in Controlled Fusion and Plasma Physics (Proc 24th Eur Conf, Berchtesgaden 1997), Vol 21A, Pt IV, European Physical Society Geneva (1997) 1413.

12. Isler, R C , McKee,G R, et al, Plasma Physics, 4 (1997) 2989.

13. Summers, H P, Atomic Data and Analysis Structure Users Manual, JET Report IR(94) 06

14. Pigarov , A Y, and Krasheninnikov, S I, Physics Letters A 222 (1996) 251.

15. Lovegrove, T, Horton, L D, Koenig,R W T, et al in Controlled Fusion and Plasma Physics (Proc 22nd Eur Conf, Bournemouth 1997), Vol 19C, Pt III, European Physical Society Geneva (1995) p301.

16. Smith, R J, Proc 8th Joint Workshop on ECE and ECRH, Max Planck Institut, IPP report III/186, 1993.
"The electron cyclotron absorption diagnostic for the JET pumped divertor plasma".

17. Borrass, K, Coster, D and Schneider, R, in Controlled Fusion and Plasma Physics (Proc 24th Eur Conf, Berchtesgaden 1997), Vol 21A, Pt IV, European Physical Society Geneva (1997) 1461.

18. Monk, R D , et al in Controlled Fusion and Plasma Physics (Proc 24th Eur Conf, Berchtesgaden 1997), Vol 21A, Pt I, European Physical Society Geneva (1997) 117.

19. Gunther,K , et al J Nucl Mater 176-177 (1990) 236.

20. Monk, R D, et al Contrib Plasma Physics 36 (1996) 37

21. Stangeby, P C, Plasma Phys and Control Fusion 37 (1995) 1337

22. Chodura, R, in Physics of Plasma Wall Interactions in Controlled Fusion, Edited by D E Post and R Behrisch, p99, Plenum Press, NewYork 1986.

23. Keilhacker,M et al Physica Scripta T2/2 (1982) 443.

24. Loarte, A, et al, submitted to Nuclear Fusion, JET preprint JET-P(97) 03

25. Stangeby, P C, Nuclear Fusion, 33(1993) 1695

26. Ghendrih, Ph, Phys. Plasmas 1 (1994) 1929.

27. Isler R C et al Phys plasmas 4 (1997) 2989.